Inorg. Chem. **2007**, *46*, 6464–6472

Synthesis, Characterization, Photophysical, and Computational Studies of Rhenium(I) Tricarbonyl Complexes Containing the Derivatives of Bipyrazine

Robert Kirgan, Megan Simpson, Curtis Moore, Jeff Day, Loan Bui, Clayton Tanner, and D. Paul Rillema*

Department of Chemistry, Wichita State University, 1845 North Fairmount Street, Wichita, Kansas 67260-0051

Received March 16, 2007

The chloro and pyridinate derivatives of rhenium(I) tricarbonyl complexes containing the diimine ligands 2,2′-bipyrazine (bpz) and 5,5′-dimethyl-2,2′-bipyrazine (Me_2bpz) are reported. Absorption maxima occur in the visible and ultraviolet regions of the spectrum; emission is structureless at room temperature and at 77 K; the infrared spectrum consists of three carbonyl stretches; electrochemically, a reversible reduction, an irreversible reduction, and an irreversible oxidation take place. Some ring protons are shielded and others deshielded in the presence of the methyl substituents attached to the bpz ring. DFT and TDDFT calculations provide insight into interpreting electronic and vibrational properties of the complexes. When compared to similar rhenium(I) tricarbonyl complexes of 2,2′-bipyridine (bpy) and 2,2′-bipyrimidine (bpm), the Me_2bpz complexes are comparable to bpm derivatives and their properties are intermediate between those of bpy and bpz complexes.

Introduction

A number of different Re(diimine)$(CO)_3$Cl, [Re(diimine)-$(CO)_3$(py)]$^+$, and [Re(diimine)$(CO)_3$(py-X)]$^+$, where X is a substituent bonded to py, complexes have been synthesized. Some rhenium(I) tricarbonyl diimine complexes have been studied for their photophysical properties,[1−22] others for solar energy conversion,[3,23−26] and others for potential applications on the basis of their emission characteristics.[27−29]

In some cases, emission from Re(I) tricarbonyl diimine complexes occurs at high energy (500−600 nm) with structure; in others, it occurs at lower energy (600−700 nm) with broad, structureless bands that are sensitive to their environment.[1,2,4−7,20] Further, changing the ancillary ligand from chloride to pyridine enhances the emission properties by increasing the emission lifetimes and emission quantum yields of the excited states. Changes in the electronic characteristics of the diimine ligand also affect the emission

* To whom correspondence should be addressed. E-mail: paul.rillema@wichita.edu.

(1) Wrighton, M.; Morse, D. L. *J. Am. Chem. Soc.* **1974**, *96*, 998.
(2) Giordano, P. J.; Wrighton, M. S. *J. Am. Chem. Soc*. **1979**, *101*, 2888.
(3) Wrighton, M. S.; Geoffroy, G. L. *Organometallic Photochemistry*; Academic Press: New York, 1979; Chapter 2.
(4) Lees, A. *Chem. Rev.* **1987**, *87*, 711.
(5) Giordano, P. J.; Fredericks, S. M.; Wrighton, M. S.; Morse, D. L. *J. Am. Chem. Soc.* **1978**, *100*, 2257.
(6) Fredericks, S. M.; Luong, J. C.; Wrighton, M. S. *J. Am. Chem. Soc*. **1979**, *27*, 7415.
(7) Smothers, W. K.; Wrighton, M. S. *J. Am. Chem. Soc*. **1983**, *105*, 1067.
(8) Vogler, A.; Kisslinger, J. *Inorg. Chim. Acta* **1986**, *115*, 193.
(9) Juris, A.; Campagna, S.; Bidd, I.; Lehn, J. M.; Zeissel, R. *Inorg. Chem*. **1988**, *27*, 4007.
(10) Van Wallendael, S.; Shaver, R. J.; Rillema, D. P.; Yoblinski, B. J.; Stathis, M.; Guarr, T. F. *Inorg. Chem*. **1990**, *29*, 1761.
(11) Sahai, R.; Rillema, D. P.; Shaver, R. J.; Van Wallendael, S.; Jackman, D. C.; Boldaji, M. *Inorg. Chem.* **1989**, *28*, 1022.
(12) Ruminski, R.; Cambron, R. T. *Inorg. Chem*. **1990**, *29*, 1574.
(13) Baiano, J. A.; Carlson, D. L.; Wolosh, G. M.; DeJesus, D. E.; Knowles, C. F.; Szabo, E. G.; Murphy, W. R., Jr. *Inorg. Chem.* **1990**, *29*, 2327.
(14) Baiano, J. A.; Kessler, R. J.; Lumpkin, R. S.; Munley, M. J.; Murphy, W. R. *J. Phys. Chem.* **1995**, *99*, 17680.
(15) Tapolsky, G.; Duesing, R.; Meyer, T. J. *J. Phys. Chem*. **1989**, *93*, 2885.
(16) Tapolsky, G.; Duesing, R.; Meyer, T. J. *Inorg. Chem*. **1990**, *29*, 2285.
(17) Lin, R.; Guarr, T. F. *Inorg. Chim. Acta* **1990**, *167*, 149.
(18) Lin, R.; Guarr, T. F.; Duesing, R. *Inorg. Chem*. **1990**, *29*, 4169.
(19) Kalyasundaram, K. *J. Chem. Soc., Faraday Trans. 2* **1986**, *82*, 2401.
(20) Sacksteder, L.; Zipp, A. P.; Brown, E. A.; Streich, J.; Demas, J. N.; DeGraff, B. A. *Inorg. Chem.* **1990**, *29*, 4335.
(21) Leasure, R. M.; Sacksteder, L.; Nesselrodt, D.; Reitz, G. A.; Demas, J. N.; DeGraff, B. A. *Inorg. Chem*. **1991**, *30*, 3722.
(22) Hino, J. K.; Della Ciana, L.; Dressicak, W. J.; Sullivan, B. P. *Inorg. Chem*. **1992**, *31*, 1072.
(23) Della Ciana, L.; Dressicak, W. J.; Sandrini, D.; Maestri, M.; Ciano, M. *Inorg. Chem*. **1990**, *29*, 2792.
(24) Meyer, T. J. *Pure Appl. Chem*. **1986**, *58*, 1193.
(25) Caspar, J. V.; Sullivan, B. P.; Meyer, T. J. *Inorg. Chem*. **1984**, *23*, 2098.
(26) Kober, E. M.; Marshall, J. L.; Dressick, W. J.; Sullivan, B. P.; Meyer, T. J. *Inorg. Chem*. **1985**, *24*, 2755.

10.1021/ic700512j CCC: $37.00
Published on Web 07/14/2007

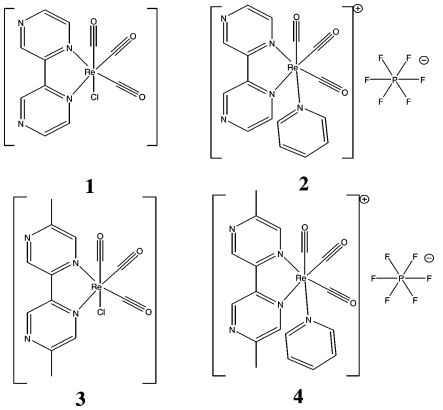

Figure 1. Schematic drawing of the complexes.

properties[30] which will be examined in this paper by way of comparing experimental to theoretical results.

The chloro and pyridinate complexes of rhenium tricarbonyl 2,2′-bipyrazine and 5,5′-dimethyl-2,2′-bipyrazine (shown in Figure 1) were investigated in this contribution. The chloride-containing bipyrazine complex was synthesized and studied before,[18,31−33] but not in great detail. The synthesis, photochemistry, crystal structures, and computational studies are presented here for all four complexes. All of these complexes have facial carbonyl groups and are luminescent at 77 K. They will be divided into two subgroups, chloride-bound and pyridine-bound and compared to analogues in the literature.

Experimental Section

Materials. The ligands 2,2′-bipyrazine[34] (bpz) and 5,5′-dimethyl-2,2′-bipyrazine[35] (Me_2bpz) were prepared as previously reported. $Re(CO)_5Cl$ was purchased from Aldrich. Optima grade methanol was purchased from Fisher Scientific, while dry acetonitrile was purchased from Sigma-Aldrich. AAPER Alcohol and Chemical Co. was the source of absolute ethanol. Tetrabutylammonium perchlorate was purchased from Southwestern Analytical Chemicals, Inc. and dried in a vacuum oven before use. Ethanol and methanol were used in a 4:1 (v/v) mixture to prepare solutions for the emission spectral and lifetime studies. Elemental analyses were obtained from M-H-W Laboratories, Phoenix, AZ.

Synthesis. Re(bpz)(CO)$_3$Cl (1). $Re(CO)_5Cl$ (0.10 g, 2.77 mmol) and bpz (0.044 g, 2.77 mmol) were mixed in a 1:1 ratio in 20 mL of ethanol. The mixture was refluxed for 3 h and allowed to cool. The mixture was slowly evaporated to yield crystals suitable for X-ray structure analysis. (Yield = 95%). Anal. Calcd for $ReC_{11}H_6N_4O_3Cl$: C, 28.48; H, 1.30; N, 12.08. Found: C, 28.55; H, 1.50; N, 11.87.

[Re(bpz)(CO)$_3$py]PF$_6$ (2). $Re(CO)_5Cl$ (0.10 g, 2.77 mmol) and $Ag(CF_3SO_3)$ (0.071 g, 2.77 mmol) were refluxed together in 20 mL of ethanol overnight. The AgCl that formed was removed by filtration, and bpz (0.044 g, 2.77 mmol) was added to the filtrate. The filtrate was heated to reflux, and then pyridine (0.022 g, 2.80 mmol) was added to the mixture. This solution was refluxed for 4 h. The volume of the solvent was then reduced to 5 mL. The mixture was added into a magnetically stirred, saturated aqueous solution of ammonium hexafluorophosphate. The solid that formed was filtered and dried. (Yield = 80%). Suitable crystals for X-ray structure analysis were obtained from slow dissolution of an ethanol solution into water. The crystals were grown in the dark to prevent photosubstitution of water. Anal. Calcd for $ReC_{16}H_{11}N_5O_3PF_6$: C, 29.45; H, 1.70; N, 10.73. Found: C, 28.71; H, 1.50; N, 10.71.

Re(Me_2bpz)(CO)$_3$Cl (3). The same procedure for the preparation of **1** was followed except that 5,5′-dimethyl-2,2′-bipyrazine (0.052 g, 2.77 mmol) was used in the place of 2,2′-bipyrazine. Upon slow evaporation of the reaction mixture, crystals suitable for X-ray structure analysis were obtained. (Yield = 95%) Anal. Calcd for $ReC_{13}H_{10}N_4O_3Cl$: C, 31.74; H, 2.05; N, 11.39. Found: C, 31.93; H, 1.97; N, 11.32.

[Re(Me_2bpz)(CO)$_3$py]PF$_6$ (4). The same procedure for the preparation of **2** was followed except 5,5′-dimethyl-2,2′-bipyrazine (0.052 g, 2.77 mmol) was used in the place of 2,2′-bipyrazine. (Yield = 80%) Anal. Calcd for $ReC_{18}H_{15}N_5O_3PF_6$: C, 31.77; H, 2.22; N, 10.29. Found: C, 31.67; H, 2.07; N, 10.20.

Computational Procedures. Calculations were affected using Gaussian '03 (rev. B.03)[36] for UNIX. The molecules were optimized using Becke's three-parameter hybrid functional B3LYP[37] with the local term of Lee, Yang, and Parr and the nonlocal term of Vosko, Wilk, and Nassiar. The basis set SDD[38] was chosen for all atoms, and the geometry optimizations were all ran in the gas phase.

(27) (a) Lo, K. K.-W.; Hui, W.-K.; Chung, C.-K.; Tsang, K. H.-K.; Lee, T. K.-M.; Li, C.-K.; Lau, J. S.-Y.; Ng, D. C.-M. *Coord. Chem. Rev.* **2006**, *250*, 1724. (b) Di Bilio, A. J.; Crane, B. R.; Wehbi, W. A.; Kiser, C. N.; Abu-Omar, M. M.; Carlos, R. M.; Richards, J. H.; Winkler, J. R.; Gray, H. B. *J. Am. Chem. Soc.* **2001**, *123*, 3181. (c) Dunn, A. R.; Belliston-Bittner, W.; Winkler, J. R.; Getzoff, E. D.; Stuehr, D. J.; Gray, H. B. *J. Am. Chem. Soc.* **2005**, *127*, 5169. (d) Saidi, M.; Seifert, S.; Kretzschmar, M.; Bergmann, R.; Pietzsch, H.-J. *J. Organomet. Chem.* **2004**, *689*, 4739. (e) Pietzsch, H.-J.; Gupta, A.; Reisgys, M.; Drews, A.; Seifert, S.; Syhre, R.; Spies, H.; Alberto, R.; Abram, U.; Schubiger, P. A.; Johannsen, B. *Bioconjugate Chem.* **2000**, *11*, 414. (f) Wei, L.; Banerjee, S. R.; Levadala, M. K.; Babich, J.; Zubieta, J. *Inorg. Chim. Acta* **2004**, *357*, 1499. (g) Jaouen, G.; Top, S.; Vessières, A.; Pigeon, P.; Leclercq, G.; Laios, I. *Chem. Commun.* **2001**, 383. (h) Zhang, J.; Vittal, J. J.; Henderson, W.; Wheaton, J. R.; Hall, I. H.; Hor, T. S. A.; Yan, Y. K. *J. Organomet. Chem.* **2002**, *650*, 123. (i) Heldt, J.-M.; Fischer-Durand, N.; Salmain, M.; Vessières, A.; Jaouen, G. *J. Organomet. Chem.* **2004**, *689*, 4775.
(28) (a) Yam, V. W.-W.; Li, B.; Yang, Y.; Chu, B. W.-K.; Wong, K. M.-C.; Cheung, K.-K. *Eur. J. Inorg. Chem.* **2003**, 4035. (b) Lundin, N.; Blackman, A.; Gordon, K.; Officer, D. *Angew. Chem., Int. Ed.* **2006**, *45*, 2582. (c) Ranjan, S.; Lin, S.-Y.; Hwang, K.-C.; Chi, Y.; Ching, W.-L.; Liu, C.-S. *Inorg. Chem.* **2003**, *42*, 1248. (d) Lee, P.-I.; Hsu, S. L.-C.; Chung, C.-T. *Synth. Met.* **2006**, *156*, 907. (e) Ng, P. K.; Gong, X.; Chan, S. H.; Lam, L. S. M.; Chan, W. K. *Chem. Eur. J.* **2001**, *7*, 4358. (f) Wang, K.; Huang, L.; Gao, L.; Jin, L.; Huang, C. *Inorg. Chem.* **2002**, *41*, 3353. (g) Lam, L. S. M.; Chan, W. K. *Chem. Phys. Chem.* **2001**, *4*, 252.
(29) (a) Yam, V. W.-W.; Ko, C.-C.; Wu, L.-X.; Wong, K. M.-C.; Cheung, K.-K. *Organometallics* **2000**, *19*, 1820. (b) Sun, S.-S.; Lees, A.; Zavalij, P. Y. *Inorg. Chem.* **2003**, *42*, 3445. (c) Sun, S.-S.; Tran, D.; Odongo, O.; Lees, A. *Inorg. Chem.* **2002**, *41*, 132. (d) Lewis, J. D.; Perutz, R. N.; Moore, J. N. *J. Phys. Chem. A* **2004**, *108*, 9037. (e) Amendola, V.; Bacchilega, D.; Costa, I.; Gianelli, L.; Montalti, M.; Pallavicini, P.; Perotti, A.; Prodi, L.; Zaccheroni, N. *J. Photochem. Photobiol. A: Chem.* **2003**, *159*, 249. (f) Lam, M. H. W.; Lee, D. Y. K.; Man, K. W.; Lau, C. S. W. *J. Mater. Chem.* **2000**, *10*, 1825. (g) Cattaneo, M.; Fagalde, F.; Katz, N. E. *Inorg. Chem.* **2006**, *45*, 6884. (h) Beer, P. D.; Timoshenko, V.; Maestri, M.; Passaniti, P.; Balzani, V. *Chem. Commun.* **1999**, 1755. (i) Curiel, D.; Beer, P. D. *Chem. Commun.* **2005**, 1909. (j) Pope, S. J. A.; Coe, B. J.; Faulkner, S. *Chem. Commun.* **2004**, 1550.
(30) Kober, E. M.; Sullivan, B. P.; Dressick, W. J.; Caspar, J. V.; Meyer, T. J. *J. Am. Chem. Soc.* **1980**, *102*, 1383.
(31) Villegas, J. M.; Stoyanov, S. R.; Huang, W.; Rillema, D. P. *Inorg. Chem.* **2005**, *44*, 2297.
(32) Kaim, W.; Kramer, H. E. A.; Vogler, C.; Rieker, J. *J. Organometallic Chem.* **1989**, *367*, 107.
(33) MacQueen, D. B.; Eyler, J. R.; Schanze, K. S. *J. Am. Chem. Soc.* **1992**, *114*, 1897.
(34) Klein, A.; Vogler, C.; Kaim, W. *Organometallics* **1996**, *15*, 236.
(35) Lafferty, J. J.; Case, F. H. *J. Org. Chem.* **1967**, *32*, 1591.
(36) Eller, C.; Smucker, B.; Eichhorn, D. M.; Rillema, D. P.; Kirgan, R. *Acta Crystallogr.* **2004**, *E60*, o433−o434.

Table 1. Crystallographic Data and Structure Refinement

complex	**1**	**2**	**3**	**4**
empirical formula	$C_{11}H_6N_4O_3ClRe$	$C_{16}H_{11}N_5O_3PF_6Re\cdot 1/2\ H_2O$	$C_{13}H_{10}N_4O_3ClRe$	$C_{18}H_{15}N_5O_3PF_6Re\cdot CH_3CN$
fw	463.85	661.47	491.90	680.52
T	150 K	150 K	150 K	150 K
λ	0.71073 Å	0.71073 Å	0.71073 Å	0.71073 Å
cryst syst	triclinic	triclinic	rhombohedral	rhombohedral
space group	$P\bar{1}$	$P\bar{1}$	$R\bar{3}$	$R\bar{3}$
unit cell dimens	$a = 6.4993(4)$ Å	$a = 8.3921(3)$ Å	$a = 27.1050(5)$ Å	$a = 33.2103(3)$ Å
	$b = 6.5962(4)$ Å	$b = 8.5622(3)$ Å	$b = 27.1050(5)$ Å	$b = 33.2103(3)$ Å
	$c = 15.2702(8)$ Å	$c = 14.5139(6)$ Å	$c = 11.2195(4)$ Å	$c = 10.6556(2)$ Å
	$\alpha = 101.790(2)°$	$\alpha = 90.727(2)°$	$\alpha = 90°$	$\alpha = 90°$
	$\beta = 92.935(3)°$	$\beta = 104.250(2)°$	$\beta = 90°$	$\beta = 90°$
	$\gamma = 102.198(2)°$	$\gamma = 95.379(2)°$	$\gamma = 120°$	$\gamma = 120°$
V	623.31(6) Å^3	1005.66(7) Å^3	7138.4(3) Å^3	10177.8(2) Å^3
Z	2	2	18	18
calcd density	2.471 g/cm^3	2.181 g/cm^3	2.060 g/cm^3	2.017 g/cm$_3$
abs coeff	9.974 mm^{-1}	6.209 mm^{-1}	7.844 mm^{-1}	5.525 mm^{-1}
F(000)	432	628	4176	5926
cryst size	0.51 × 0.16 × 0.08 mm^3	0.30 × 0.20 × 0.10 mm^3	0.21 × 0.16 × 0.14 mm^3	0.12 × 0.12 × 0.08 mm^3
cryst habit	needle	prism	prism	needle
cryst color	lustrous dark red	clear light red	clear intense orange	clear intense orange
θ range for data collection	3.22−26.00°	1.45−25.99°	3.62−25.99°	3.19−25.99°
limiting indices	$-8 \le h \le 7$	$-10 \le h \le 10$	$-33 \le h \le 32$	$-40 \le h \le 40$
	$-8 \le k \le 8$	$-10 \le k \le 10$	$-33 \le k \le 33$	$-40 \le k \le 40$
	$-18 \le l \le 18$	$-17 \le l \le 17$	$-13 \le l \le 13$	$-12 \le l \le 13$
reflns collected/ unique	17 236/2430	17 584/3959	38 984/3070	93 689/4407
	[R(int) = 0.0265]	[R(int) = 0.0215]	[R(int) = 0.0604]	[R(int) = 0.0874]
completeness to $\theta = 26.00$	99.9%	99.9%	98.4%	99.3%
refinement method	full-matrix least-squares on F^2			
data/restraints/ params	2430/0/181	3959/0/298	3070/0/201	4407/2/319
refinement threshold	$I > 2\sigma(I)$	$I > 2\sigma(I)$	$I > 2\sigma(I)$	$I > 2\sigma(I)$
data > threshold	2375	3831	2738	3627
GOF on F^2	1.089	1.093	1.121	1.054
final R indices	R1 = 0.0100	R1 = 0.0161	R1 = 0.0238	R1 = 0.0233
[$I > 2\sigma(I)$]	wR2 = 0.0247	wR2 = 0.0383	wR2 = 0.0394	wR2 = 0.0503
R indices	R1 = 0.0106	R1 = 0.0171	R1 = 0.0290	R1 = 0.0344
(all data)	wR2 = 0.0251	wR2 = 0.0386	wR2 = 0.0401	wR2 = 0.0534
largest diff. peak and hole	0.363 and −0.495 e.A^{-3}	0.851 and −0.508 e.A^{-3}	0.652 and −1.385 e.A^{-3}	1.012 and −0.590 e.A^{-3}

Nonequilbrium TDDFT[39]/CPCM[40] calculations were employed to produce a number of singlet excited states[41] in acetonitrile based on the optimized geometry in the gas phase. The calculation is nonequilbrium with respect to the polarization of the solvent reaction field and the electronic state of the input. For singlet excited states, this is the singlet ground state.[42] All oscillator values and singlet and triplet excited-state values are presented in the Supporting Information S1−4. The simulated absorption spectra were run in the solvent acetonitrile to match experimental conditions. All vibrational analyses revealed no negative frequencies and were run in the gas phase only.

X-ray Analysis. The crystal was affixed to a nylon cryoloop using oil (Paratone-n, Exxon) and mounted in the cold stream of a Bruker Kappa-Apex-II area-detector diffractometer.[43a] The temperature at the crystal was maintained at 150 K using a Cryostream

(37) Frisch, M. J.; Trucks, G. W.; Schlegel, H. B.; Scuseria, G. E.; Robb, M. A.; Cheeseman, J. R.; Montgomery, J. A., Jr.; Vreven, T.; Kudin, K. N.; Burant, J. C.; Millam, J. M.; Iyengar, S. S.; Tomasi, J.; Barone, V.; Mennucci, B.; Cossi, M.; Scalmani, G.; Rega, N.; Petersson, G. A.; Nakatsuji, H.; Hada, M.; Ehara, M.; Toyota, K.; Fukuda, R.; Hasegawa, J.; Ishida, M.; Nakajima, T.; Honda, Y.; Kitao, O.; Nakai, H.; Klene, M.; Li, X.; Knox, J. E.; Hratchian, H. P.; Cross, J. B.; Bakken, V.; Adamo, C.; Jaramillo, J.; Gomperts, R.; Stratmann, R. E.; Yazyev, O.; Austin, A. J.; Cammi, R.; Pomelli, C.; Ochterski, J. W.; Ayala, P. Y.; Morokuma, K.; Voth, G. A.; Salvador, P.; Dannenberg, J. J.; Zakrzewski, V. G.; Dapprich, S.; Daniels, A. D.; Strain, M. C.; Farkas, O.; Malick, D. K.; Rabuck, A. D.; Raghavachari, K.; Foresman, J. B.; Ortiz, J. V.; Cui, Q.; Baboul, A. G.; Clifford, S.; Cioslowski, J.; Stefanov, B. B.; Liu, G.; Liashenko, A.; Piskorz, P.; Komaromi, I.; Martin, R. L.; Fox, D. J.; Keith, T.; Al-Laham, M. A.; Peng, C. Y.; Nanayakkara, A.; Challacombe, M.; Gill, P. M. W.; Johnson, B.; Chen, W.; Wong, M. W.; Gonzalez, C.; Pople, J. A. *Gaussian 03*, revision B.04; Gaussian, Inc.: Wallingford, CT, 2004.

(38) (a) Becke, A. D. *J. Chem. Phys*. **1993**, *98*, 5648. (b) Lee, C.; Yang, W.; Parr, R. G. *Phys. Rev. B* **1988**, *37*, 785. (c) Vosko, S. H.; Wilk, L.; Nusair, M. *Can. J. Phys*. **1980**, *58*, 1200. (d) Andrae, D.; Hauessermann, U.; Dolg, M.; Stoll, H.; Preuss, H. *Theor. Chim. Acta* **1990**, *77*, 123.

(39) (a) Stratmann, R. E.; Scuseria, G. E.; Frisch, M. J. *J. Chem. Phys*. **1998**, *109*, 8218. (b) Bauernschmitt, R.; Ahlrichs, R. *Chem. Phys. Lett*. **1996**, *256*, 454. (c) Casida, M. E.; Jamorski, C.; Casida, K. C.; Salahub, D. R. *J. Chem. Phys*. **1998**, *108*, 4439.

(40) (a) Cossi, M.; Barone, V. *J. Chem. Phys*. **2001**, *115*, 4708. (b) Barone, V.; Cossi, M. *J. Phys. Chem. A* **1998**, *102*, 1995. (c) Cossi, M.; Rega, N.; Scalmani, G.; Barone, V. *J. Comput. Chem*. **2003**, *24*, 669.

(41) The CPCM is designed to account for the bulk physical properties of the solvent. It does not account for specific solvent−solute interactions. The TDDFT is known to perform well for the computing of charge-transfer excited states between closely spaced moieties. The tandem use of CPCM and TDDFT is currently the most suitable computational approach for the treatment of the solvent effects to the transition metal complexes excited-state energies.

(42) Frisch, Æ.; Frisch, M. J.; Trucks, G. W. *Gaussian 03 User's Reference, version 7.0*; Gaussian, Inc.: Carnegie, PA, 2003; p 206.

(43) (a) *APEX2 User Manual*; Bruker AXS Inc.: Madison, WI, 2006. (b) Sheldrick, G. M. *SHELXS97 and SHELXL97*; University of Göttingen: Göttingen, Germany, 1997.

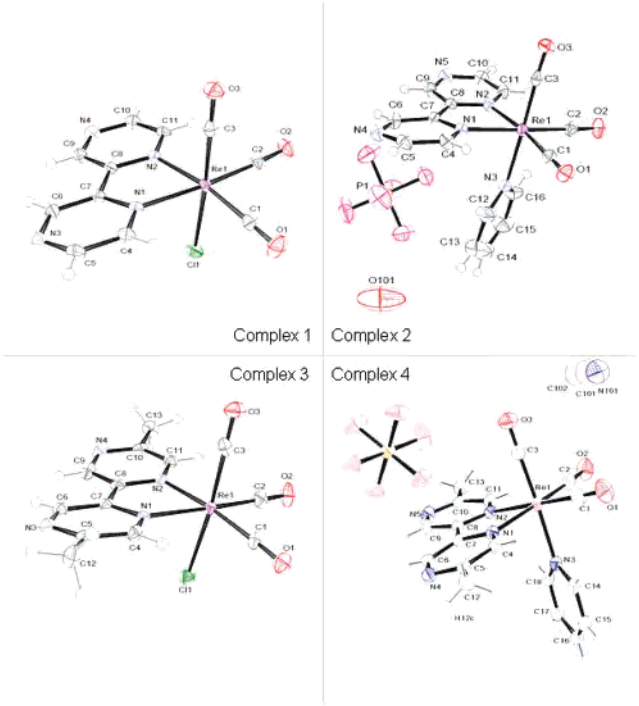

Figure 2. ORTEP figures with thermal ellipsoids drawn at the 50% probability level.[40]

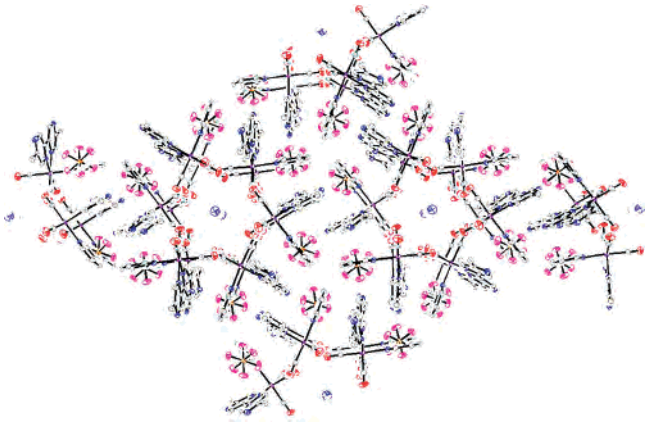

Figure 3. Crystal packing for complex **4** as seen down the 001 face.

700EX Cooler (Oxford Cryosystems). The unit cell was determined from the setting angles of 218 reflections collected in 36 frames of data. Data were measured with a redundancy of 6.2 using a CCD detector at a distance of 50 mm from the crystal with a combination of θ and ω scans. A scan width of 0.5° and a time of 10 s were employed along with graphite-monochromated M Kα radiation (λ = 0.71073 Å) that was collimated to a 0.6 mm diameter. Data collection, reduction, structure solution, and refinement were performed using the Bruker Apex2 suite (v2.0−2).[43a] All available reflections to $2\theta_{max} = 52°$ were harvested and corrected for Lorentz and polarization factors with Bruker SAINT (v6.45).[43a] Reflections were then corrected for absorption, interframe scaling, and other systematic errors with SADABS 2004/1. The structure was solved (direct methods) and refined (full-matrix least-squares against F2) with the Bruker SHELXTL package (v6.14−1).[43b] All non-hydrogen atoms were refined using anisotropic thermal parameters. All hydrogen atoms were included at idealized positions and not refined.

Physical Measurements. Absorption measurements were determined with a HP8452A diode array spectrophotometer, and data

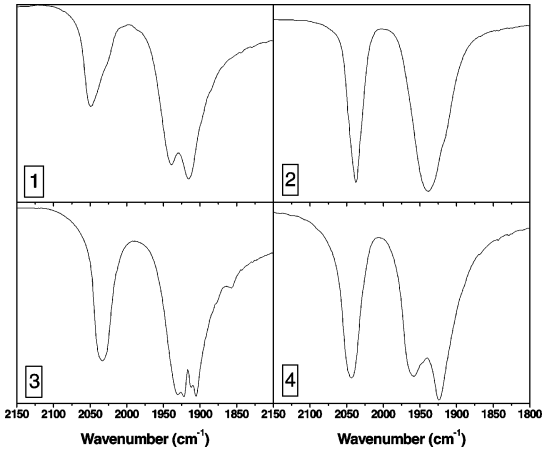

Figure 4. IR spectra of the carbonyl stretch region.

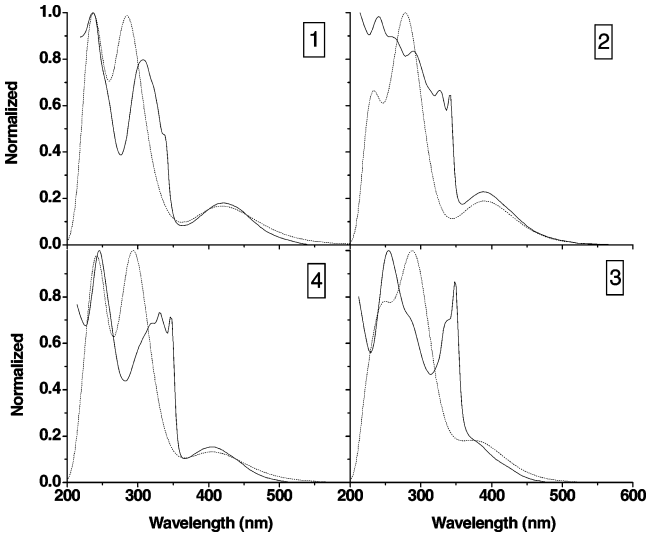

Figure 5. Experimental spectra (−) and corrected calculated spectra (− − −) in acetonitrile.

were acquired with OLIS Global works software. All extinction coefficients were determined in acetonitrile from Beer's Law. Fluorescence measurements were obtained with a Spex Fluorolog 2:1:2 spectrophotometer. The solvent for both room temperature and 77 K studies was a fresh solution of 4:1 ethanol/methanol. All samples were degassed using the freeze−pump−thaw method three or four times; residual gas had a pressure of ∼150 mTorr. The absorbance was set to 0.1 at the λ_{max} for complexes **1**−**3** and at 374 nm for complex **4**. All NMR spectra were obtained on a Varian 400 MHz spectrometer. The solvent was DMSO with TMS as an internal standard. A Nicolet Avatar 360 FTIR was utilized to gather IR data. The samples were pressed into a KBr pellet and ran with an instrument resolution of 4 cm^{-1}.

Cyclic voltammograms were obtained in acetonitrile with 0.1 M tetrabutylammonium perchlorate ($TBAClO_4$) as the supporting electrolyte. A platinum metal disk was used for the working electrode, and a platinum wire functioned as the auxiliary electrode. All voltammograms were recorded versus a Ag/AgCl electrode. A PAR EG&G (Model 263A) potentiostat/galvanostat was used to obtain the data, and the PAR data interpreting program was used to process the data.

Results

Crystal Structures. Crystallographic data and structure refinement data for complexes **1**−**4** are listed in Table 1,

Table 2. Calculated vs X-ray Bond Distances (Å) and Selected Angles (deg)

	1			3		
complex	X-ray	calcd	difference	X-ray	calcd	difference
Re−N(L)	2.150	2.178	0.028	2.158	2.181	0.023
Re−N(L)	2.151	2.178	0.027	2.177	2.181	0.004
Re−C_{Ax}	1.902	1.927	0.025	1.924	1.925	0.001
Re−C_{Eq}	1.917	1.942	0.025	1.922	1.940	0.018
Re−C_{Eq}	1.937	1.942	0.005	1.917	1.940	0.023
Re−Cl	2.484	2.550	0.066	2.460	2.550	0.090
(L)N−Re−N(L)	75.21	75.18	−0.04	75.34	75.20	−0.14
C−Re−N(L)	98.17	96.91	−1.26	99.60	96.96	−2.91
C−Re−C	89.86	90.33	0.47	87.85	90.33	2.48
	2			**4**		
complex	X-ray	calcd	difference	X-ray	calcd	difference
Re−N(L)	2.161	2.189	0.028	2.160	2.191	0.031
Re−N(L)	2.162	2.189	0.027	2.178	2.191	0.013
Re−N(Py)	2.202	2.250	0.048	2.213	2.251	0.038
Re−C_{Ax}	1.920	1.951	0.031	1.944	1.949	0.005
Re−C_{Eq}	1.927	1.944	0.017	1.929	1.943	0.014
Re−C_{Eq}	1.933	1.944	0.011	1.916	1.943	0.027
(L)N−Re−N(L)	75.03	75.09	0.06	75.08	75.20	0.12
C−Re−N(L)	96.38	97.29	0.91	99.77	97.20	−2.57
C−Re−C	90.02	90.20	0.18	90.08	90.31	0.23

and ORTEP diagrams are shown in Figure 2. The bpz-containing complexes crystallized in the $P\bar{1}$ space group, whereas the Me_2bpz-containing complexes packed in the $R\bar{3}$ space group (Table 1). It is unclear why such a simple change in the ligand caused the difference in the crystal space groups for these complexes. As shown in the packing diagram in Figure 3 for **4**, six molecules form a six-cornered "star" with an acetonitrile molecule in the center in the $R\bar{3}$ space group. There are three molecules on top and three on bottom, and they alternate around the "star." The carbonyl groups make up the inner part and the PF_6^- anions are tucked into the pocket between each cation.

Molecular Structures. Selected bond distances and angles are listed in Table 2. With the exception of one bond length (Re−C_{Eq}), complex **1** has shorter R−-ligand bond lengths than its counterpart, complex **2**. Similarly, with the same exception, complex **3** had shorter bond lengths than its counterpart, complex **4**. A comparison of Re−C bond lengths for complexes **3** and **4** to complexes **1** and **2**, respectively, revealed that one Re−C_{Eq} bond distance is longer by ∼0.01 Å, the other Re−C_{Eq} bond distance is approximately the same length, but the Re−C_{Ax} bond distance is longer by ∼0.02 Å.

Nuclear Magnetic Resonance Studies. NMR data and assignments of protons are given in Table 3, and their designations are outlined in the figure below the table. The proton resonances of the pyridine ligand (protons 5, 6, and 7) were found upfield from those of the bipyrazine ligand (protons 1, 2, and 3). The resonance for proton 1 is shifted downfield for Re(Me_2bpz)$(CO)_3$Cl compared to proton 1 for Re(bpz)$(CO)_3$Cl; proton 3, on the other hand, is shifted upfield. The methyl groups attached to the bpz ring alter the ring current causing deshielding of proton 3 and shielding of proton 1. Replacement of Cl^- by pyridine in both bpz and Me_2bpz complexes gives rise to the same observation, proton 1 is shifted downfield and proton 3 is shifted upfield. The shift for proton 1 is greatest for the pyridine adducts; the methyl groups attached to bipyrazine cause the greatest shift for proton 3. The inductive affect of the methyl groups also causes a downfield shift of proton 5 for the pyridinate complexes.

Infrared Studies. The energy of the carbonyl stretches for complexes **1**−**4** are listed in Table 4, and the spectra are shown in Figure 4. As typical for rhenium(I) tricarbonyl complexes, three bands were observed, although for complex **2** only a shoulder was discernible on the low-energy absorption manifold. For the pyridinate adducts, the bands for complex **2** shift to lower energy compared to complex **1**, but the absorption maxima for complex **4** shifts to higher energy compared to complex **3**.

Absorption Studies. Absorption maxima and absorption coefficients are listed in Table 5, and absorption spectra are shown in Figure 5. Metal-to-ligand charge-transfer bands (MLCT) are assigned to the low-energy absorptions and $\pi \rightarrow \pi^*$ to the absorptions at higher energy.[44] Absorption coefficients for the complexes range from 3240 to 4020 M^{-1} cm^{-1} for the MLCT region and from 10 540 to 20 540 M^{-1} cm^{-1} for the $\pi \rightarrow \pi^*$ region. The MLCT maxima of the pyridine adducts were blue-shifted with respect to their chloride derivatives and have higher absorption coefficients.

Table 3. NMR Data with Assignment of Protons

	proton						
complex	1	2	3	4	5	6	7
1	9.01, d, (J = 2.8 Hz)	9.15, dd (J = 3.2, 1.2 Hz)	10.17, d, (J = 1.2 Hz)				
2	9.15, d, (J = 3.2 Hz)	9.39, d, (J = 3.0, 1.0 Hz)	10.09, d, (J = 3.2 Hz)		8.47, d, (J = 4.8 Hz)	7.44, t, (J = 7.6 Hz)	7.99, t, (J = 7.2 Hz)
3	9.03, s		9.97, d, (J = 1.6 Hz)	2.74, s			
4	9.28, s		9.89, d, (J = 1.6 Hz)	2.79, s	8.54, dd, (J = 6.4, 1.2 Hz)	7.45, t, (J = 7.6 Hz)	7.99, t, (J = 7.0 Hz)

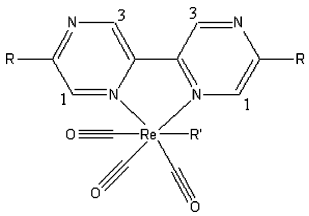

R = H (2), CH_3 (4)

R' = Cl,

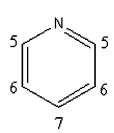

Table 4. Experimental, Calculated, and Corrected Carbonyl Stretch Frequencies (cm^{-1})

	exptl	calcd	corrected		exptl	calcd	corrected
1	2049.0	1984.4	2026.7	**3**	2033.3	1981.6	2023.2
	1939.0	1911.2	1936.3		1922.1	1906.5	1930.5
	1915.8	1886.0	1905.3		1905.4	1881.7	1899.9
2	2037.2	2004.4	2051.3	**4**	2043.2	2001.7	2048.0
	1938.3	1925.8	1954.3		1957.9	1920.7	1948.1
	–	–	–		1924.1	1916.3	1942.6

Table 5. Absorption Energies (nm) and Assignments (Values in Parenthesis Are Extinction Coefficients)

	type of transition					
	$\pi \rightarrow \pi^*$			MLCT		
1	236		308	336		420
	(17 090)		(13 730)	(8340)		(3240)
2	240	262	290	326	342	388
	(16 130)	(14 640)	(13650)	(10 920)	(10 540)	(3740)
3	246		320	330	346	404
	(20 540)		(14 200)	(15 090)	(14 700)	(3340)
4		254	282	336	348	374sh
		(12 050)	(8750)	(8430)	(10 430)	(4020)

Table 6. Emission Maxima Obtained by Excitation at the MLCT Maxima and Excitation Maxima Obtained from Excitation Spectra

	$\lambda_{ex,\ 298\ K}$	$\lambda_{ex,\ 77\ K}$	$\lambda_{em,298\ K}$	$\lambda_{em,\ 77\ K}$	$\Phi \times 10^3$	$\tau_{298\ K,\ ns}$	$\tau_{77\ K,\ ns}$
1	336, 423	339, 401	705	656	0.09	na	98
2	340, 392, 419	341, 390	684	632	1.72	25	1522
3	346, 402, 423	348, 397	718	641	0.73	na	2537
4	349, 390	349, 385	669	617	8.94	95	5507

For the rhenium(I) Me_2bpz derivatives, the absorption spectra are less resolved, particularly for complex **2** in the ultraviolet region and for complex **4** in the MLCT region. Three of the four complexes show a unique, very sharp peak at around 350 nm. The reason for this peak is unknown, but it is often observed in rhenium tricarbonyl complexes.

Emission. The emission spectra were obtained at both room temperature and 77 K in 4:1 EtOH/MeOH. The emission maxima are listed in Table 6 along with emission quantum yields and emission lifetimes. The room-temperature emission spectra were very weak in intensity, so all quantum yields are multiplied by 1000. Complexes **3** and **4** have larger quantum yields than their counterpart complexes **1** and **2**, respectively. According to the quantum yields, complex **4** is the most intense and complex **1** is the weakest emitter at room temperature. When the temperature of the solution was lowered to 77 K, the emission bands shifted ~50 nm to higher energy and the emission intensity increased by a factor of 4−5.

Figure 6 shows normalized emission spectra at 77 K. The general shape remained the same for all four complexes, and no structure was observed. Further discussion about emission properties will be given below.

Cyclic Voltammetry. Oxidation−reduction processes were determined by cyclic voltammetry, and potentials are listed in Table 7. Two reductions and one oxidation were observed. The first reduction was reversible and assigned to reduction of the bpz ligand. The second reduction was irreversible and assigned to reduction of rhenium(I).[45] An irreversible oxidation assigned to $Re^{+} \rightarrow Re^{2+}$ was also observed.[45] The first reduction and oxidation become more negative for the dimethylated bipyrazine derivatives due to the electron-donating characteristics of the methyl substituents but more positive with replacement of chloride ion with pyridine.

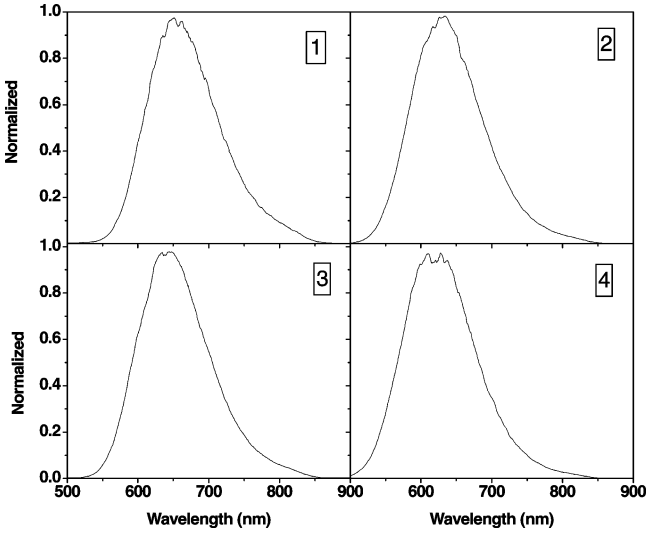

Figure 6. Emission spectra at 77 K excited at the MLCT maxima.

Table 7. Oxidation and Reduction Potentials vs Ag/AgCl

complex	$E_{1/2}$(V) $LL^{0/-}$	E_p(V) $Re^{+/0}$	E_p(V) $Re^{2+/+}$
1	−0.76	−1.29	1.56
2	−0.60	−1.30	2.07
3	−0.94	−1.31	1.52
4	−0.79	−1.27	2.01

Discussion

Calculated Structures. As shown in Table 2, all the calculated bond distances were longer than those determined by X-ray analysis which is common among metal complexes. The difference averaged 1.88 pm for all bonds except the rhenium−chloride bonds which averaged 6.5 pm. Bond distances were also calculated for the analogues Re(bpy)$(CO)_3$Cl, Re(bpm)$(CO)_3$Cl, $[Re(bpy)(CO)_3(py)]^+$, and $[Re(bpm)(CO)_3(py)]^+$, where bpy is 2,2′-bipyridine and bpm is 2,2′-bipyrimidine. All the calculated coordinates are listed in the Supporting Information (S1−4). The practice of using these minimized structures for DFT and TDDFT calculations has been followed to obtain molecular orbitals, their energies, and molecular properties.

Molecular Orbitals. Figure 7 shows a graphical representation of the HOMO and LUMO for each of the complexes, and Table 8 lists the distribution of electron density in the molecules. The HOMO for the chloro complexes contain ~40% d_{Re} character with an equal distribution of electron density (~40%) on Cl^- and the

(44) Stoyanov, S. R.; Villegas, J. M.; Cruz, A. J.; Lockyear, L. L.; Reibenspeis, J. H.; Rillema, D. P. *J. Chem. Theory Comput.* **2005**, *1*, 95.

(45) Lin, R.; Fu, Y.; Brock, C. P.; Guarr, T. F. *Inorg. Chem.* **1992**, *31*, 4346.

(46) Shaver, R. J.; Perkovic, M. W.; Rillema, D. P.; Woods, C. *Inorg. Chem.* **1995**, *34*, 5446.

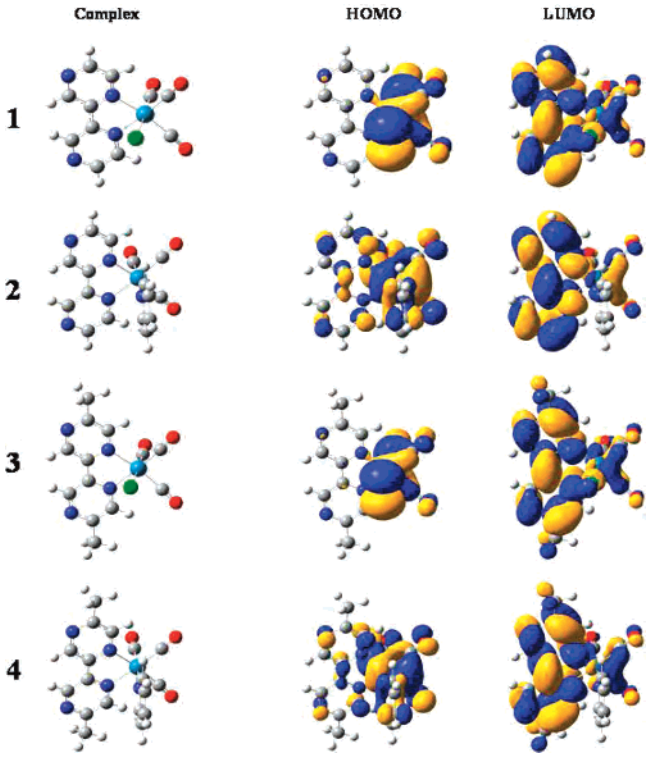

Figure 7. Graphical representation of optimized structure, HOMO and LUMO orbital diagrams.

Table 8. Electron Distribution in % within the Rhenium(I) Molecules and the Mulliken Charges

	HOMO				LUMO				
complex	Re	CO	ring	Cl	Re	CO	ring	Cl	MC
bpy	41	19	1	39	2	4	93	1	0.454
bpm	40	19	1	40	2	4	93	1	0.500
bpz	40	18	1	41	3	5	90	2	0.475
Me_2bpz	40	18	1	41	3	5	90	2	0.463
	Re	CO	ring	py	Re	CO	ring	py	
bpy	63	24	8	5	2	4	93	1	0.826
bpm	63	24	8	5	2	4	93	1	0.884
bpz	63	23	8	6	4	5	91	1	0.849
Me_2bpz	63	24	8	5	3	5	91	1	0.841

remainder on the CO ligands. The HOMO of the pyridinate complexes contain ~60% d_{Re} character with ~20% of the electron density located on the CO ligands and the remainder equally distributed over the pyridine and bipyrazine ligands. The electron density on the LUMO, LUMO+1, and LUMO+2 in all cases is centered on the bipyrazine ligand (90%).

The electron distribution and energies of bpy and bpm analogues were also determined for comparison to the bpz and Me_2bpz complexes. Details for these results are located in the Supporting Information section S5. Similar electron distributions were found within the Cl and py series for all the complexes.

Mulliken charges on the rhenium center are also listed in Table 8. The charge nearly doubles from 0.5 for the chloro complexes to 0.8 for the pyridinate species. The Mulliken charge is greatest for the bpz and bpm complexes in accord with the greater π-backbonding associated with these ligands.

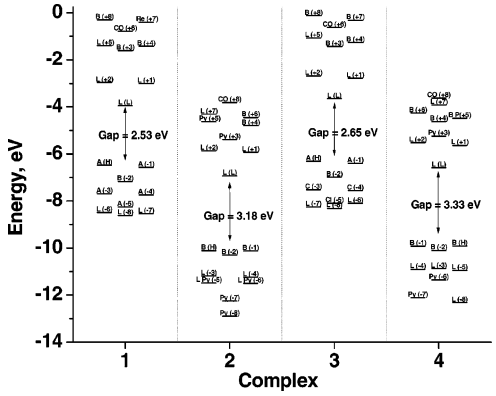

Figure 8. Molecular orbital energy diagram for nine frontier occupied orbitals and nine frontier virtual orbitals of the complexes in the singlet ground state in the gas phase. A = Re/CO/Cl, B = Re/CO, C = Re/Cl, L = Ligand, Py = Pyridine.

Table 9. Experimental MLCT, Calculated MLCT, and Corrected Values (nm)

	MLCT		
complex	λ_{exptl}	λ_{calcd}	λ_{corr}
1	420	476	419
2	388	439	390
3	404	458	405
4	374	417	373

Molecular Orbital Energies. The energies of nine frontier occupied orbitals and nine frontier virtual orbitals for all four complexes are shown in Figure 8. The energy gap for complexes **1** and **3** is ~2.6 eV; for complexes **2** and **4**, it is ~3.3 eV. These values correlate nicely with the absorption spectra MLCT maxima.

The energy gaps for the chloro complexes Re(bpy)$(CO)_3$Cl, Re(bpm)$(CO)_3$Cl, Re(bpz)$(CO)_3$Cl, and Re(Me_2-bpz)$(CO)_3$Cl follow the series Re(bpy)$(CO)_3$Cl (2.80 eV) > Re(bpm)$(CO)_3$Cl ≈ Re(Me_2bpz)$(CO)_3$Cl (2.65 eV) > Re-(bpz)$(CO)_3$Cl (2.53 eV). For the pyridine complexes, the energy gaps fell in the series: $[Re(bpy)(CO)_3(py)]^+$ (3.46 eV) > $[Re(Me_2bpz)(CO)_3(py)]^+$ (3.33 eV) > $[Re(bpm)(CO)_3$-$(py)]^+$ (3.31 eV) > $[Re(bpz)(CO)_3(py)]^+$ (3.18 eV).

Absorption Spectra. After correction, absorption spectra as shown in Figure 5 gave good overlap for the calculated and experimental MLCT energy manifolds. A plot of the experimental MLCT maxima versus the calculated MLCT maxima was linear. The intercept was used to correct the calculated values, which are listed in Table 9 along with the experimental and calculated energies. All simulated spectra were determined in the gas phase and acetonitrile; the results obtained in acetonitrile were chosen for comparison.

The MLCT transition observed in the absorption spectra for complexes **1** and **3** occurs from the HOMO−1 to the LUMO level. Whereas the MLCT absorption manifold for complexes **2** and **4** consists of transitions from two identical sets of orbitals separated by ~600 cm^{-1}, the HOMO−2 and HOMO, to the LUMO. These optical transitions are best labeled metal-ligand-to-ligand charge transfer (MLLCT).

Infrared Vibrational Spectra. The vibrational spectra were calculated as described in the Experimental Section and are listed in Table 4. The values were all lower in energy then the experimentally determined ones. The values were

Table 10. Carbonyl Stretch Frequency (cm^{-1}) Comparisons for **1**−**4** and Similar Compounds

$Re(CO)_3(bpy)Cl$[44]	$Re(CO)_3(bpm)Cl$[46]	$Re(CO)_3(bpz)Cl$	$Re(CO)_3(Me_2bpz)Cl$
2022	2033	2049	2033
(sh)	1906(sh)	1939	1922
1890	1899	1916	1905
$[Re(CO)_3(bpy)(py)]^{+}$[45a]	$[Re(CO)_3(bpm)(py)]^{+}$[46b]	$[Re(CO)_3(bpz)(py)]^{+b}$	$[Re(CO)_3(Me_2bpz)\ (py)]^{+b}$
2026	2043(sh)	2037	2043
(sh)	2033		1958
1906	1916	1938	1924

[a] $CF_3SO_3^-$ salt. [b] PF_6^- salt.

corrected by potting the energies of the experimental carbonyl stretches versus the calculated values, yielding a linear relationship. The intercepts of the lines were used to obtain the corrected values which were in closer agreement with the experimental determinations.

The calculated spectrum yielded some valuable information on the origin of the stretches. There are three different stretches: a symmetric stretch which involves all three carbonyl groups, an asymmetric stretch that also involves all three carbonyl groups, and a third asymmetric stretch involving only the equatorial carbonyl groups. The lowest energy vibration for the two chloro complexes is an asymmetric stretch involving all three carbonyl groups. The middle vibration involves two carbonyl groups and the highest energy vibration is the symmetric stretch involving all three carbonyl groups. For the pyridine-bound complexes, the two lower-energy vibrations switch places. The middle vibration becomes the asymmetric stretch involving all three carbonyl groups, and the lowest energy vibration involves two carbonyl groups.

A listing of carbonyl vibrational frequencies for various diimine complexes is given in Table 10. The order of frequencies for the chloro complexes is bpz > bpm ≈ Me_2-bpz > bpy; the order for the py complexes is Me_2bpz ≈ bpm > bpz > bpy. Complexes of bpm and Me_2bpz seem to approximate each other in this comparison.

Nuclear Magnetic Resonance. The electron density present on the bpz ring in the HOMO orbital primarily resides on the 2, 4, and 6 positions, leaving the 3 and 5 positions with much less. Consequently, the influence of the methyl group located in position 5 on the ring system causes shielding of proton 3 with little effect on the proton in position 6. Addition of pyridine has a similar effect on the proton located in the 3 position but results in deshielding of protons in the 5 and 6 positions of the bipyrazine rings. Hence, the resonance from these proton moves downfield.

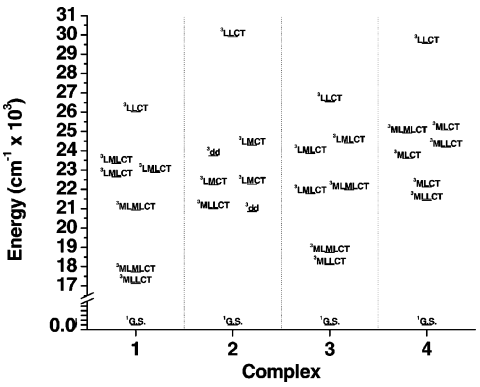

Figure 9. Calculated Triplet Excited States Relative to Ground States.

Table 11. Experimental, Calculated, and Corrected Emission Energies (nm)

	chloride derivatives			
	exptl	calcd	corrected	% error
bpy	521	500	524	0.64%
bpm	584	532	582	0.28%
bpz	656	584	677	3.14%
Me_2bpz	641	552	619	3.49%
	pyridine derivatives			
	exptl	calcd	corrected	% error
bpy	495	427	496	0.25%
bpz	632	480	642	1.55%
Me_2bpz	617	467	606	1.77%

Emission. Emission energies were calculated for the chloro and pyridinate complexes and are tabulated in Table 11, and an energy level scheme is shown for the bpz complexes in Figure 9. Plots of the calculated vs the experimental emission energies yielded intercepts which were used to determine corrected energies that are also listed in Table 10. The corrected values were similar to the experimentally determined values.

The emission lifetimes were short at room temperature compared to rhenium(I) bipyridine tricarbonyl derivatives.[1] The decay at room temperature can be related to the energy gap law, in part, since the energy gaps for $[Re(bpy)(CO)_3(py)]^+$ (λ_{em} = 556 nm) and $[Re(bpy)(CO)_3(Cl)$ (λ_{em} = 595 nm) are large compared to those of the complexes examined here.

At 77 K, however, the emission lifetimes of $[Re(bpy)(CO)_3(py)]^+$ and $[Re(Me_2bpz)(CO)_3(py)]^+$ were comparable, while the emission lifetimes of $[Re(bpm)(CO)_3(py)]^+$ and $[Re(bpz)(CO)_3(py)]^+$ were 3−4 times less. This suggests that a thermally activated nonradiative decay process occurs at room temperature but not at 77 K.

Cyclic Voltammetry. We have previously reported[47] that the first oxidation can be correlated with the HOMO orbital energy to yield a straight line. Plots of E_p vs the HOMO energy for the complexes studied here along with data for $Re(bpy)(CO)_3Cl$,[44] $[Re(bpy)(CO)_3py]^+$,[44] $Re(bpm)(CO)_3Cl$,[46] and $[Re(bpm)(CO)_3py]^+$,[46] where bpm is 2,2′-bipyrimidine were linear, as shown in Figure 10. Plots of the reduction potential versus the LUMO energies are also linear.

(47) Stoyanov, S. R.; Villegas, J. M.; Rillema, D. P. *Inorg. Chem.* **2002**, *41*, 2941.

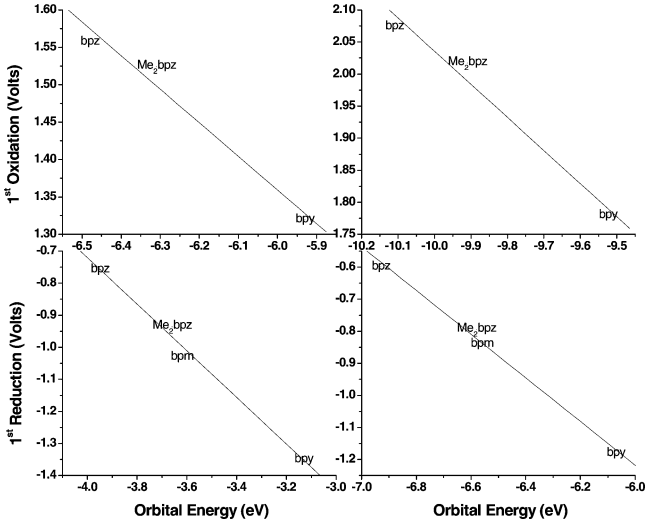

Figure 10. Correlation charts of HOMO vs first Oxidation and LUMO vs first Reduction. Left: chloride-containing compounds. Right: pyridine-containing compounds. Potentials are vs Ag/AgCl.

Conclusion

Four new rhenium complexes containing two ligands, 2,2′-bipyrazine and 5,5′-dimethyl-2,2′-bipyrazine, have been described. Synthesis and spectroscopic and computational studies were performed and analyzed. The dimethyl bipyrazine ligand behaved electronically like a 2,2′-bipyrimidine ring. The lifetime and quantum yields were greater for the methyl bipyrazine derivatives, as well as blue-shifts observed in the absorption spectra. The larger quantum yields and remote nitrogen atoms could make these complexes useful for attachment to surfaces for solar energy conversion devices.

Acknowledgment. We thank the support from the Department of Education for Graduate Assistance in Areas of National Need grant, the Wichita State University High Performance Computing Center, the Wichita State University Office of Research Administration, and the Department of Energy for support.

Supporting Information Available: Cartesian coordinates and triplet TDDFT transitions for all eight complexes; TDDFT singlet transitions and detailed orbital distributions for the four bpz complexes; a full calculated bond length comparison, calculated CO stretches, frontier orbitals (all eight complexes), and triplet transitions (all eight complexes); and correction curves used to correct some of the data. This material is available free of charge via the Internet at http://pubs.acs.org.

IC700512J